to possess. However, even if they are implicit, schemas are an economical way to characterize the gradual acquisition of an organized framework of associative "semantic-like" information from "episodic-like" events that, once acquired, allows relevant new information to be assimilated and stored rapidly. Given that animals have daily activities such as finding food and water, it is important for them to retain an organized body of knowledge about where these may be found and to be able to update such a framework rapidly, within one trial. This inferential flexibility of rodent cognition is now established in several domains (*9*).

References and Notes

1. F. C. Bartlett, *Remembering* (Cambridge Univ. Press, Cambridge, 1932).
2. K. Craik, *The Nature of Explanation* (Cambridge Univ. Press, Cambridge, 1943).
3. J. D. Bransford, *Human Cognition: Learning, Understanding and Remembering* (Wadsworth, Belmont, CA, 1979).
4. P. N. Johnson-Laird, *Mental Models: Towards a Cognitive Science of Language, Inference, and Consciousness* (Cambridge Univ. Press, Cambridge, 1983).
5. J. D. Bransford, M. K. Johnson, *J. Verb. Learn. Verb. Behav.* **11**, 717 (1972).
6. E. A. Maguire, C. D. Frith, R. G. M. Morris, *Brain* **122**, 1839 (1999).
7. J. O'Keefe, L. Nadel, *The Hippocampus as a Cognitive Map* (Clarendon, Oxford, 1978).
8. B. O. McGonigle, M. Chalmers, *Nature* **267**, 694 (1977).
9. H. Eichenbaum, *Neuron* **44**, 109 (2004).
10. L. R. Squire, *Psychol. Rev.* **99**, 195 (1992).
11. Y. Dudai, R. G. M. Morris, in *Brain, Perception and Memory: Advances in Cognitive Sciences*, J. Bolhuis, Ed. (Oxford Univ. Press, Oxford, 2001), pp. 147–162.
12. J. L. McClelland, B. L. McNaughton, R. C. O'Reilly, *Psychol. Rev.* **102**, 419 (1995).
13. M. Day, R. F. Langston, R. G. M. Morris, *Nature* **424**, 205 (2003).
14. M. Bunsey, H. Eichenbaum, *Nature* **379**, 255 (1996).
15. R. P. Kesner, M. R. Hunsaker, P. E. Gilbert, *Behav. Neurosci.* **119**, 781 (2005).
16. S. Wirth *et al.*, *Science* **300**, 1578 (2003).
17. K. Sakai, Y. Miyashita, *Nature* **354**, 152 (1991).
18. Y. Miyashita, *Science* **306**, 435 (2004).
19. B. Bontempi, C. Laurent-Demir, C. Destrade, R. Jaffard, *Nature* **400**, 671 (1999).
20. P. W. Frankland, B. Bontempi, *Nat. Rev. Neurosci.* **6**, 119 (2005).
21. H. Eichenbaum, P. Dudchenko, E. Wood, M. Shapiro, H. Tanila, *Neuron* **23**, 209 (1999).
22. The food used as one member of each PA (diet pellets manufactured in a range of different flavors) was hidden in a sand mixture that had been adulterated by ground-up pellets consisting of 1% of each of the six flavors used on any daily session (6% total). This and other procedures masked any olfactory cue that might have guided the animals to the correct sand well. The animals were shown to use recall of spatial location exclusively in making their sand-well choices. No food pellets were present in the sand mixture during nonrewarded probe tests.
23. See supporting material on *Science* Online.
24. S. M. Zola-Morgan, L. R. Squire, *Science* **250**, 288 (1990).
25. J. J. Kim, M. S. Fanselow, *Science* **256**, 675 (1992).
26. S. G. Anagnostaras, S. Maren, M. S. Fanselow, *J. Neurosci.* **19**, 1106 (1999).
27. P. J. Bayley, J. J. Gold, R. O. Hopkins, L. R. Squire, *Neuron* **46**, 799 (2005).
28. T. Maviel, T. P. Durkin, F. Menzaghi, B. Bontempi, *Science* **305**, 96 (2004).
29. H. F. Harlow, *Psychol. Rev.* **56**, 51 (1949).
30. E. Teng, L. R. Squire, *Nature* **400**, 675 (1999).
31. T. J. Teyler, P. DiScenna, *Behav. Neurosci.* **100**, 147 (1986).
32. G. Buzsaki, *Neuroscience* **31**, 551 (1989).
33. A. G. Siapas, M. A. Wilson, *Neuron* **21**, 1123 (1998).
34. B. L. McNaughton *et al.*, in *Sleep and Synaptic Plasticity*, C. Smith, P. Maquet, Eds. (Oxford Univ. Press, New York, 2003), pp. 225–246.
35. R. G. Morris, *Eur. J. Neurosci.* **23**, 2829 (2006).
36. R. C. O'Reilly, J. W. Rudy, *Psychol. Rev.* **108**, 311 (2001).
37. K. A. Norman, R. C. O'Reilly, *Psychol. Rev.* **110**, 611 (2003).
38. A. Pasupathy, E. K. Miller, *Nature* **433**, 873 (2005).
39. R. S. Rosenbaum, G. Winocur, M. Moscovitch, *Behav. Brain Res.* **127**, 183 (2001).
40. M. Moscovitch, L. Nadel, G. Winocur, A. Gilboa, R. S. Rosenbaum, *Curr. Opin. Neurobiol.* **16**, 179 (2006).
41. R. G. M. Morris, F. Schenk, F. Tweedie, L. E. Jarrard, *Eur. J. Neurosci.* **2**, 1016 (1990).
42. H. Eichenbaum, C. Stewart, R. G. M. Morris, *J. Neurosci.* **10**, 3531 (1990).
43. G. Winocur, M. Moscovitch, S. Fogel, R. S. Rosenbaum, M. Sekeres, *Nat. Neurosci.* **8**, 273 (2005).
44. J. J. Bolhuis, C. A. Stewart, E. M. Forrest, *Q. J. Exp. Psychol. B* **47**, 129 (1994).
45. R. J. Sutherland *et al.*, *Hippocampus* **11**, 27 (2001).
46. R. E. Clark, N. J. Broadbent, L. R. Squire, *Hippocampus* **15**, 260 (2005).
47. S. J. Martin, L. de Hoz, R. G. M. Morris, *Neuropsychologia* **43**, 609 (2005).
48. R. G. M. Morris, P. Garrud, J. N. Rawlins, J. O'Keefe, *Nature* **297**, 681 (1982).
49. F. Vargha-Khadem *et al.*, *Science* **277**, 376 (1997).
50. M. Mishkin, W. A. Suzuki, D. G. Gadian, F. Vargha-Khadem, *Philos. Trans. R. Soc. London Ser. B* **352**, 1461 (1997).
51. P. J. Bayley, L. R. Squire, *J. Neurosci.* **22**, 5741 (2002).
52. D. O. Hebb, *The Organization of Behaviour* (Wiley, New York, 1949).
53. U. Frey, R. G. M. Morris, *Nature* **385**, 533 (1997).
54. A. Govindarajan, R. J. Kelleher, S. Tonegawa, *Nat. Rev. Neurosci.* **7**, 575 (2006).
55. W. T. Greenough, J. E. Black, in *Developmental Behavioral Neuroscience*, M. R. Gunnar, C. A. Nelson, Eds., vol. 24 of *Minnesota Symposia on Child Psychology* Erlbaum, Hillsdale, NJ, 1992); pp. 155–200.

56. Supported by a UK Medical Research Council program grant (R.G.M.M.), a UK Biotechnology and Biological Sciences Research Council studentship award (R.F.L.), and a Fondation pour la Recherche Médicale fellowship (I.B.). We thank J. Tulloch for assistance with the histology.

Supporting Online Material
www.sciencemag.org/cgi/content/full/316/5821/76/DC1
Materials and Methods
Figs. S1 to S8
Tables S1 and S2
References

5 October 2006; accepted 23 February 2007
10.1126/science.1135935

REPORTS

Nonstoichiometric Dislocation Cores in α-Alumina

N. Shibata,[1]* M. F. Chisholm,[2] A. Nakamura,[3] S. J. Pennycook,[2] T. Yamamoto,[4] Y. Ikuhara[1]

Little is known about dislocation core structures in oxides, despite their central importance in controlling electrical, optical, and mechanical properties. It has often been assumed, on the basis of charge considerations, that a nonstoichiometric core structure could not exist. We report atomic-resolution images that directly resolve the cation and anion sublattices in alumina (α-Al_2O_3). A dissociated basal edge dislocation is seen to consist of two cores; an aluminum column terminates one partial, and an oxygen column terminates the second partial. Each partial core is locally nonstoichiometric due to the excess of aluminum or oxygen at the core. The implication for mechanical properties is that the mobile high-temperature dislocation core structure consists of two closely spaced partial dislocations. For basal slip to occur, synchronized motion of the partials on adjacent planes is required.

The core structures of dislocations are critical to the electronic, optical, and mechanical properties of a wide range of materials. For most simple monometallic crystals, dislocation core termination can be determined; however, in complex crystals such as oxides, either cation or anion columns (or both) can be the terminating atomic columns even with the same dislocation character (i.e., characteristic displacement vectors called Burgers vectors, **b**). The possibility of nonstoichiometric cores also arises but has usually been rejected because it suggests the possibility of charged dislocations (*1*, *2*) and the presence of long-range Coulomb fields with a high associated electrostatic energy. This has been suggested to be the reason why the close-packed {111} crystal plane in alkali halides cannot be an easy slip system (*2*, *3*). Detailed knowledge of dislocation core structures and compositions is critical to understand dislocations in ionic crystals.

[1]Institute of Engineering Innovation, University of Tokyo, 2-11-16, Yayoi, Bunkyo, Tokyo 113-8656, Japan. [2]Materials Science and Technology Division, Oak Ridge National Laboratory, Oak Ridge, TN 37831–6030, USA. [3]Department of Intelligent Materials Engineering, Osaka City University, 3-3-138, Sugimoto, Sumiyoshi-ku, Osaka, 558-8585, Japan. [4]Department of Advanced Materials Science, University of Tokyo, 5-1-5, Kashiwanoha, Kashiwa, Chiba 277-8561, Japan.

*To whom correspondence should be addressed. E-mail: shibata@sigma.t.u-tokyo.ac.jp

The inherent structural complication of alpha alumina (α-Al_2O_3) and, indeed, other complex compounds has led to conflicting models for dislocation glide (*4–6*). Alumina is widely used in many industrial areas because of its superior mechanical, thermal, and chemical stability at high temperatures. Slip on the {0001} basal plane is reported to be the dominant deformation system at elevated temperatures (*7*), and thus important for understanding the high-temperature mechanical behavior. Kronberg (*4*) first proposed a basal dislocation slip model based on structurally related hexagonal metals. Slip was assumed to occur between Al and O basal-plane layers. To maintain the normal octahedral coordination of the oxygen to aluminum sites, Kronberg proposed the synchroshear mechanism, whereby two shears operate in different directions on adjacent atomic planes. This mechanism has been shown to operate in the Laves phase compound $HfCr_2$ (*8*). Later, Bilde-Sørensen *et al*. (*5*) argued that the slip between Al and O planes would require charge transport. Alternatively, they proposed that dislocation slip would occur along the midplane on the puckered Al (cation) layer. They argued that this choice of the slip plane allows the moving dislocations to carry no net charge.

Figure 1A shows a ball-and-stick model of α-Al_2O_3 in the $\langle 1\bar{1}00\rangle$ projection. From this viewing direction, Al- and O-atom sites are arranged as distinct columns. The stacking sequence of α-Al_2O_3 along the $\langle 0001\rangle$ direction consists of 12 alternating cation and anion basal layers. The cation layers are slightly puckered along the $\langle 0001\rangle$ direction. Bilde-Sørensen *et al*. proposed that basal slip occurs between these shifted Al sites (*5*).

The core structure of a basal edge dislocation in α-Al_2O_3 is observed by scanning transmission electron microscopy (STEM). Now, sub-angstrom resolution can be achieved with this technique (*9*). Figure 1, B and C, show simultaneous high-angle annular dark-field (HAADF) and bright-field STEM images of α-Al_2O_3 viewed along the $\langle 1\bar{1}00\rangle$

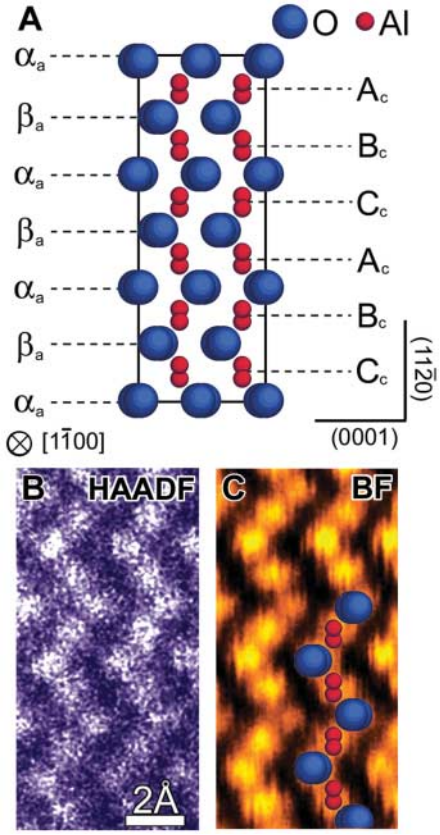

Fig. 1. Crystal structure and simultaneous atomic-resolution high-angle annular dark-field (HAADF) and bright-field (BF) STEM images of α-Al_2O_3. (**A**) Unit structure of α-Al_2O_3 viewed from the $\langle 1\bar{1}00\rangle$ direction. The structure of α-Al_2O_3 consists of alternating Al and O planes along the $\langle 0001\rangle$ direction, whose stacking sequence is $\cdot\cdot\alpha_a A_c \beta_a B_c \alpha_a C_c \beta_a A_c \alpha_a B_c \beta_a C_c \alpha_a \cdot\cdot$. From the $\langle 1\bar{1}00\rangle$ projection, we can distinguish individual Al and O columns. (**B** and **C**) Simultaneous HAADF (B) and bright-field (C) STEM images of α-Al_2O_3 viewed from the $\langle 1\bar{1}00\rangle$ direction. Comparison of the images shows that the bright spots in the bright-field image directly correspond to the positions of atomic columns under the conditions used to obtain the images (*11*). As seen in the images, bright-field STEM can distinguish Al and O atomic columns in this projection.

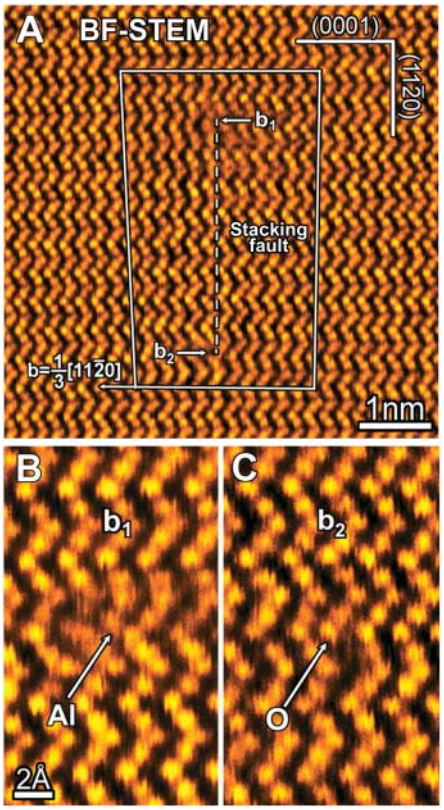

Fig. 2. Atomic-resolution bright-field STEM image of a basal edge dislocation core in α-Al_2O_3. (**A**) Typical core structure of a basal dislocation observed from the $\langle 1\bar{1}00\rangle$ direction. The dislocation core is dissociated with two partials ($\frac{1}{3}\langle 10\bar{1}0\rangle$ and $\frac{1}{3}\langle 01\bar{1}0\rangle$) connected by a $\{11\bar{2}0\}$ stacking fault. (**B** and **C**) Bright-field STEM images of the upper and lower partial dislocation cores, respectively. The upper partial core is terminated by an Al column, whereas the lower partial core is terminated by an O column. Both core terminations lie in between the Al and O atomic planes. Each partial core is nonstoichiometric due to the excess of Al or O, but the total basal dislocation chemically preserves Al_2O_3 stoichiometry.

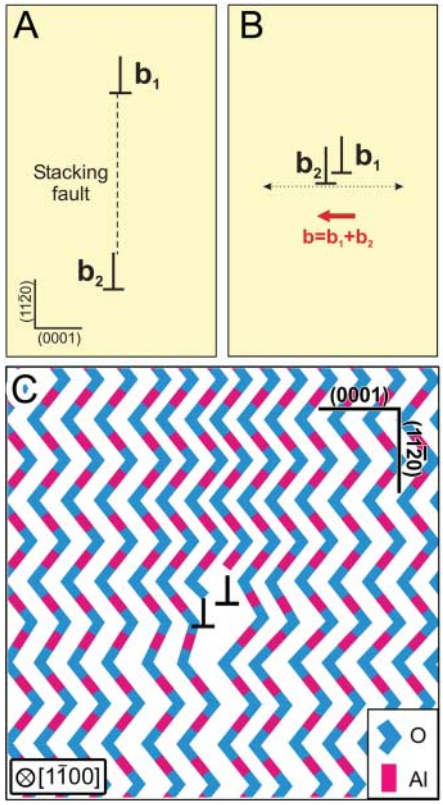

Fig. 3. Schematics of basal edge dislocation core structures observed at low temperatures and the mobile core at high temperatures. (**A**) Schematic illustration of basal edge dislocation core structure observed in this study. The perfect basal edge dislocation dissociates into two partial dislocations perpendicular to the slip plane with the formation of a $\{11\bar{2}0\}$ stacking fault in between. (**B**) Schematic illustration of mobile basal edge dislocation core model at high temperatures. Two partials move very close together without forming a $\{11\bar{2}0\}$ stacking fault in between. (**C**) Proposed atomic structure model ($\langle 1\bar{1}00\rangle$ projection) of mobile perfect basal edge dislocation at high temperatures, based on the present low-temperature observations. Blue and red segments in the figure correspond to the O and Al atomic columns, respectively. In this model, the two dissociated partials observed at low temperature are located on adjacent basal planes in the mobile high-temperature dislocation.

direction. The Z-contrast image obtained with the HAADF detector is an incoherent image (*10*); it is essentially a map of the scattering power of the specimen. There is a direct correspondence between the features in the specimen and their image. In contrast, the phase-contrast image obtained with a small bright-field detector has coherent image characteristics, which is comparable to the parallel beam high-resolution TEM. The contrast is influenced by the focus of the objective lens and specimen thickness, orientation, and scattering power. This makes phase-contrast images of unknown structures difficult to directly interpret. However, this sensitivity can be exploited to provide much greater contrast variations than can be obtained from the Z-contrast images of low–atomic number elements (such as Al and O). The simultaneously recorded Z- and phase-contrast images (Fig. 1, B and C) of the $\langle 1\bar{1}00\rangle$ projection of α-Al_2O_3 reveal parallel kinked lines of spots that reflect the arrangement of alternating O and Al columns along the $\langle 0001\rangle$ direction. Under the conditions used to obtain these two images, the bright features of the Z-contrast image are seen to correspond to the bright features in the bright-field image. These bright features identify the positions of the two O columns and the puckered Al column in each segment of the kinked lines seen in this projection (*11*).

Figure 2A shows a typical bright-field STEM image of a basal dislocation core in α-Al_2O_3. The line direction of the dislocation is parallel to the observing direction, so that the core structure is set at an "edge-on" condition. In this condition, bright spots in the image correspond to the positions of atomic columns as determined from the simultaneous Z-contrast image. It is apparent that at room temperature, this dislocation is not a single perfect dislocation ($\mathbf{b} = \frac{1}{3}\langle 11\bar{2}0\rangle$), but has an extended structure with partials ($\mathbf{b} = \frac{1}{3}\langle 10\bar{1}0\rangle$ and $\mathbf{b} = \frac{1}{3}\langle 01\bar{1}0\rangle$) connected by a $\{11\bar{2}0\}$ stacking fault, consistent with the previous reports of dislocation observations after basal slip deformation (*12–14*). The dissociation is considered to be driven by the reduction of strain energy and suppressed by increasing stacking-fault energy. Dissociation occurs on the $\{11\bar{2}0\}$ plane by self-climb (*14*). No evidence for dissociation on the $\{0001\}$ basal plane is observed. Our low-temperature observations show that the cores are separated in the $\langle 11\bar{2}0\rangle$ direction by only 0.24 nm. This observation is consistent with stacking-fault energy calculations that show that the $\{0001\}$ fault has higher energy than the $\{11\bar{2}0\}$ fault at low temperatures (*15*).

The bright-field STEM images of each dissociated partial core are shown in Fig. 2, B and C. The arrows in the images indicate the respective position of an extra half-plane termination of the two partials. The images reveal that the upper core is terminated between vertices of the kinked line of atoms at an Al-column position, whereas the lower core is terminated at a vertex of the kinked line of atoms at an O-column position. These observations clearly show both dislocation core terminations and, thus, indicate that the slip planes of the dislocations are located between the Al and O atomic planes. Moreover, the partials terminated by Al or O column indicate that the partial cores are locally not stoichiometric. Contrary to the common assumption, nonstoichiometric core structures actually exist in an ionic crystal. Although each partial dislocation core is nonstoichiometric, the total dislocation preserves Al_2O_3 stoichiometry.

Because the dissociation occurs in the direction normal to the $\{0001\}$ slip plane, as in Fig. 3A, glide of the dissociated dislocations on the $\{0001\}$ planes would require continuous structural rearrangements as the stacking fault between the partials is moved. In this case, dislocation motion would require atomic diffusion and would be very sluggish at low temperatures. It is thus expected that the dislocations that are mobile at high temperatures are not dissociated with a $\{11\bar{2}0\}$ stacking fault (*13*, *14*), as schematically shown in Fig. 3B. That is, the mobile dislocation core at high temperature should consist of two closely spaced partial dislocations. At the most basic level, dislocation glide occurs by the successive slip of terminating atomic columns on the stationary atomic planes. In α-Al_2O_3, the relative motions of $\{0001\}$ O layers and the sandwiched Al layer are considered to be involved in the basal dislocation glide. The difference in core termination results in two slightly different slip processes. If the dislocation is O terminated, the moving O plane slips over an Al plane. If, instead, the dislocation is Al terminated, the moving Al plane slips over an O plane. On the basis of our low-temperature observations, we propose that the slip planes of moving partials are located not on the same atomic plane, but on adjacent Al and O $\{0001\}$ planes. Figure 3C shows the possible perfect basal edge dislocation core structure mobile at high temperatures. We assume that the two dissociated partials observed at low temperature are located on adjacent basal planes in the mobile high-temperature dislocation. Although other reconstructions are possible, our observations show that these Al- and O-terminated partials exist, and when the dislocation glide stops, this model can dissociate by climb to form partial dislocation core structures consistent with our experimental observation. Thus, we propose that the atomic-scale basal slip processes are based on the simple core model shown in Fig. 3C. Because the schematic is viewed in a $\langle 1\bar{1}00\rangle$ projection, the vector component normal to the schematic is not shown. However, it should be stated that the two partials have equal and opposite vector components normal to the schematic.

Figure 4, A to C, shows the slip sequence of the core model shown in Fig. 3C. The partial dislocations ($\mathbf{b} = \frac{1}{3}\langle 10\bar{1}0\rangle$ and $\mathbf{b} = \frac{1}{3}\langle 01\bar{1}0\rangle$) combine to produce a unit dislocation ($\mathbf{b} = \frac{1}{3}\langle 11\bar{2}0\rangle$). Again, only the slip components perpendicular to the $\langle 1\bar{1}00\rangle$ projection are shown in this schematic. The successive slip of the two partials on adjacent planes (slip planes 1 and 2) recovers the perfect stacking sequence on the Al sublattice (*11*). However, in sapphire, there is a slight deviation from the perfect close-packed structure seen in the oxygen

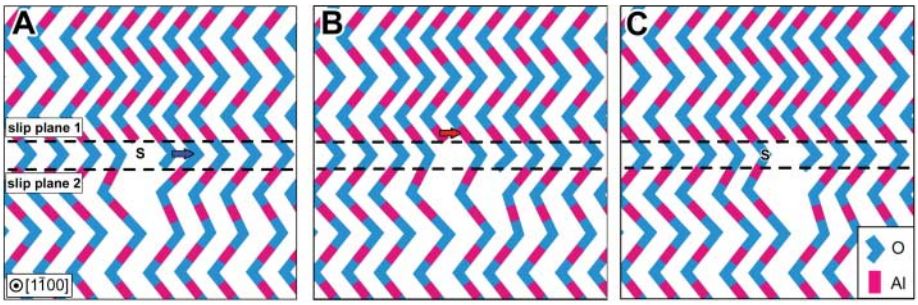

Fig. 4. Schematics of the mobile high-temperature basal edge dislocation core structure in cross section ($\langle 1\bar{1}00\rangle$ projection). Blue and red segments in the figure correspond to the O and Al atomic columns, respectively. (**A**) The dislocation, consisting of adjacent partial dislocations with O and Al termination. The slip planes of the two partials are on adjacent atomic planes (slip planes 1 and 2). "s" indicates the initial position of the dislocation. In these schematics, only the vector components perpendicular to the viewing direction are shown, but the two partials actually have equal and opposite vector components perpendicular to the schematic. (**B**) The first partial (O-terminated) slipping on a fixed Al plane. (**C**) The passage of the second partial (Al-terminated) slipping on an O plane. It is expected that (B) and (C) occur simultaneously, and during the process, slight relaxation in the O plane in between the slip planes 1 and 2 is required to preserve the perfect stacking sequence in O layers. The plain-view schematics of the present basal dislocation motion show that the proposed dislocation motion preserves a perfect stacking sequence in Al layers (*11*).

sublattice that is correlated with the stacking of adjacent Al layers (*16*). This slight deviation in oxygen positions can be schematically seen in the projected structure model of Fig. 1A. If these deviations were a spatially fixed part of the structure, the motion of a single partial would result in a stacking fault in the oxygen sublattice. In the present slip model, the O plane in between slip planes 1 and 2 is sheared by only one partial, and thus a stacking fault on the O sublattice would be produced if we assume rigid O layers. However, the deviations are related to the positions of the Al atoms, neighboring O, atoms and vacant sites sandwiched between the O layers. Because the perfect Al stacking is preserved after the dislocation motion, the O sublattice can also preserve a perfect stacking sequence by an appropriate small modification in the O atom positions. It is important to note that these two partial motions are not independent in our proposed model. Both partials move simultaneously on adjacent {0001} basal planes to complete the perfect dislocation slip. A total basal dislocation is thus considered to possess two atomic slip planes. This core structure is expected to dissociate after the dislocation stops moving and form two partials, consistent with our observations in Fig. 2.

We propose that basal slip in α-Al_2O_3 is controlled by the partial dislocations that dissociate from the perfect $\frac{1}{3}\langle 11\bar{2}0\rangle$ dislocation. The structure of these partials is based on our low-temperature observations, in which each partial core is terminated by Al and O columns, respectively, but the total dislocation preserves Al_2O_3 stoichiometry. Bilde-Sørensen *et al*. (*5*) also proposed a stoichiometric core model, but the slip plane (located at the midplane on the puckered Al layer) is not consistent with our images. Our images clearly show that the termination of both partials is located in between the Al and O layers at low temperature. Our results represent a definitive starting point for realistic atomic-level modeling of slip processes, dislocation generation, and their effects on the mechanical properties of α-Al_2O_3. Also, the present results will provide a crucial check for future theoretical calculations of dislocations in complex oxides.

We have provided experimental evidence that locally nonstoichiometric structures are allowed in crystals with strong ionic character. Simultaneous HAADF and bright-field STEM imaging with aberration correction is a powerful tool for observing such localized defect structures, even in very complex crystals. The possibility for atomic-scale characterization of dislocation core structures will assist our understanding of dislocation activity and its effects on the electrical, optical, and mechanical properties of complex, multicomponent materials.

References and Notes

1. J. P. Hirth, J. Lothe, *Theory of Dislocations* (Krieger, Malabar, FL, ed. 2, 1992).
2. R. W. Whitworth, *Adv. Phys.* **24**, 203 (1975).
3. J. J. Gilman, *Acta Metall.* **7**, 608 (1959).
4. M. L. Kronberg, *Acta Metall.* **5**, 507 (1957).
5. J. B. Bilde-Sørensen *et al*., *Acta Mater.* **44**, 2145 (1996).
6. D. E. Luzzi, G. Rao, T. A. Dobbins, D. P. Pope, *Acta Mater.* **46**, 2913 (1998).
7. K. P. D. Lagerlöf, A. H. Heuer, J. Castaing, J. P. Rivière, T. E. Mitchell, *J. Am. Ceram. Soc.* **77**, 385 (1994).
8. M. F. Chisholm, S. Kumar, P. Hazzledine, *Science* **307**, 701 (2005).
9. P. D. Nellist *et al*., *Science* **305**, 1741 (2004).
10. S. J. Pennycook, D. E. Jesson, *Phys. Rev. Lett.* **64**, 938 (1990).
11. Materials and Methods are available as supporting material on *Science* Online.
12. T. E. Mitchell, B. J. Pletka, D. S. Phillips, A. H. Heuer, *Philos. Mag.* **34**, 441 (1976).
13. A. Nakamura, T. Yamamoto, Y. Ikuhara, *Acta Mater.* **50**, 101 (2002).
14. K. P. D. Lagerlöf *et al*., *Acta Metall.* **32**, 97 (1984).
15. P. R. Kenway, *Philos. Mag. B* **68**, 171 (1993).
16. S. Geschwind, J. P. Remeika, *Phys. Rev.* **122**, 757 (1961).

17. We thank K. P. D. Lagerlöf for valuable discussions. This research was supported by the Japan Society for the Promotion of Science and the Division of Materials Sciences and Engineering, Office of Basic Energy Sciences, U.S. Department of Energy.

Supporting Online Material

www.sciencemag.org/cgi/content/full/316/5821/82/DC1
Materials and Methods
Figs. S1 and S2
References

11 October 2006; accepted 14 February 2007
10.1126/science.1136155

Acid Catalysis in Basic Solution: A Supramolecular Host Promotes Orthoformate Hydrolysis

Michael D. Pluth, Robert G. Bergman,* Kenneth N. Raymond*

Although many enzymes can promote chemical reactions by tuning substrate properties purely through the electrostatic environment of a docking cavity, this strategy has proven challenging to mimic in synthetic host-guest systems. Here, we report a highly charged, water-soluble, metal-ligand assembly with a hydrophobic interior cavity that thermodynamically stabilizes protonated substrates and consequently catalyzes the normally acidic hydrolysis of orthoformates in basic solution, with rate accelerations of up to 890-fold. The catalysis reaction obeys Michaelis-Menten kinetics and exhibits competitive inhibition, and the substrate scope displays size selectivity, consistent with the constrained binding environment of the molecular host.

Synthetic chemists have long endeavored to design host molecules capable of selectively binding slow-reacting substrates and catalyzing their chemical reactions. Whereas synthetic catalysts are often site-specific and require certain properties of the substrate to insure catalysis, enzymes are often able to modify basic properties of the bound substrate such as pK_a (where K_a is the acid dissociation constant) in order to enhance reactivity. Two common motifs used by nature to activate otherwise unreactive compounds are the precise arrangement of hydrogen-bonding networks and electrostatic interactions between the substrate and adjacent residues of the protein (*1*). Precise arrangement of hydrogen bonding networks near the active sites of proteins can lead to well-tuned pK_a matching (*2*) and can result in pK_a shifts of up to eight units, as shown in bacteriorhodopsin (*3*). Similarly, purely electrostatic interactions can greatly favor charged states and have been responsible for pK_a shifts of up to five units for acetoacetate decarboxylase (*4*). Attempts have been made to isolate the contributions of electrostatic versus covalent interactions to such pK_a shifts; however, this remains a difficult challenge experimentally. This challenge emphasizes the importance of synthesizing host molecules that, like enzyme cavities, can enhance binding of small molecular guests and, in a few cases, catalyze chemical reactions (*5*–*9*).

Supramolecular assemblies with available functional groups have been used to generate solution-state pK_a shifts of up to two pK_a units (*10*–*13*) and to catalyze chemical reactions (*14*, *15*). Synthetic hosts often rely on hydrogen bonding or ion-dipole interactions for guest inclusion, and numerous studies have investigated the effects of charge on guest binding affinities in supramolecular host-guest systems (*16*, *17*). We report here a synthetic supramolecular host assembly that relies exclusively on electrostatic and hydrophobic interactions for thermodynamic stabilization of protonated

Department of Chemistry, University of California, Berkeley, Berkeley, CA 94720, USA.

*To whom correspondence should be addressed. E-mail: rbergman@berkeley.edu (R.G.B.); raymond@socrates.berkeley.edu (K.N.R.)